A LANDCOVER CLASSIFICATION SCHEME FOR HIGH RESOLUTION IMAGERY AND IT'S APPLICATION TO BUSHFIRE PROTECTION IN RESIDENTIAL AREAS

J. R. Kim [a, *], J.-P Muller [a]

[a] Dept. of Space and Climate Physics, University College London, Holmbury St. Mary, Dorking, Surrey, RH5 6NT, UK jk2@mssl.ucl.ac.uk

ABSTRACT:

With the increasing degree of global climate change, bushfires are becoming a major threat to human life and property. A risk assessment of bushfires is dependent on the availability of suitable information on the environment and human activities. Most of the spatial information for fire behaviour prediction is time-dependent, so it is both quite difficult and potentially very expensive to maintain and ensure the reliability of such data. A suitable source of wide coverage is high resolution (≤1m) satellite imagery for risk assessment in bushfire areas. Our objective is to exploit high-resolution stereo data such as IKONOS and extract all possible information such as the vertical dimensions of a forest, the crown size and shape of some individual trees, the location of tree and grass areas, the topography of bare land and the location of housing areas. This was achieved by extracting a DSM, DTM and landcover from IKONOS stereo multispectral imagery. Then we employed FARSITE (Fire Area Simulator http://www.farsite.org) to simulate fire behaviour with several different ignition points in order to assess the risk to housing within residential areas which can be detected by our classification scheme. This case study shows how high resolution stereo images can be exploited to cope with a natural disaster by extracting detailed information on both the natural and man-made environment.

1. BACKGROUND

Recently bushfires have become one of the major targets of remote sensing research through early warning systems developed for medium resolution satellite data and prediction and hazard assessment systems implemented for bushfires. The latter parts are subject to human activity and time dependent environments (e.g. tree crown and human residence information) so there is strong demand for active and updated GIS construction. According to Chen and McAneney (2003), bushfires can penetrate into residential areas from the bushland-urban interface at distances up to 700 metres. This means, that a time dependent landscape database construction is crucial for bushfire protection and decision making. Since ground surveys for this purpose are high cost, high resolution satellite imagery analysis is proposed as an alternative method. There are several methods which have sought to classify residential area's landcover or even to detect individual trees or building objects. Moreover, recent research work to construct DTMs, which is indispensable for hazard assessment and behaviour prediction of bushfire, from high resolution 3D range data have shown good enough quality for such application. In this work, we apply landcover classification as well as DTM extraction by combining multi-spectral imagery and stereo IKONOS in order to extract geo-spatial information. This is then input into a third party fire simulator which is called FARSITE to yield risk maps dependent on the location of simulated (or real) fire locations. Using this method, the potential of high resolution satellite imagery for hazard assessment and fire behaviour prediction for a bushfire can be assured. The main technological challenge of this research is the extraction of reliable topographic information and landcover classification. To address this need we developed and have exploited a multi stage DSM-DTM extractor and classifier fusing 3D range data with multi-spectral imagery.

2. DATA SETS AND TEST AREA DESCRIPTION

The test data employed here is the IKONOS stereo and multi-resolution images provided by the ISPRS (http://www.isprs.org/data/ikonos_hobart/) over the area surrounding Hobart ,Tasmania, Australia where bushfires continue to pose a significant risk, especially due to the severe drought conditions at present. These data consist of one stereo image pair and multi-spectral IKONOS imagery. In addition, the University of Melbourne provided GPS measurements for GCP setting.

In 1967, the Tasmanian fire claimed 52 lives and destroyed 1400 homes in the Hobart area within a single day (Emergency Management Australia 2006a). More recently, a bushfire in 1998 burned 30 square km in the Hobart area (Emergency Management Australia 2006b). During summer and autumn seasons, the hot and dry weather in Southern Australia (Bureau of Meteorology Australia, 2003) causes the grass and forest to be tinder-dry so there is a high probability that any bushfire will threaten the suburban areas of Hobart as it is a mixture of houses and bushland.

An auxiliary data set of a 9 second resolution (approximately 250m) DTM of the Hobart area (Geoscience Australia, 2005) was employed for initial image rectification and eventual stereo DTM verification.

3. ALGORITHMS AND PROCESSING

Firstly, the IKONOS sensor information was updated using GCPs which were provided by the University of Melbourne. Then a multi-stage stereo image matcher consisting first of an image matcher exploiting the epi-polarity of an IKONOS stereo pair, and then using an Adaptive Least Squared Correlation (ALSC) was applied. Improved sensor information is used to define a search area within the epi-polar rectified image. The subsequent IKONOS stereo DEM was then used for the

construction of a bare earth DTM through a hierarchical slope analysis and then combined with multi-spectral data. Then by fusing the IKONOS multi-spectral information with a normalised DEM (DEM-DTM), a fine resolution classification was performed. In this manner tree, grass and some residential areas are identified. In addition, large sized building and tree footprints can be individually reconstructed. For better individual landcover object identification, which is less influenced by topography and illumination conditions, a classification scheme based on a FCFM (Looney, 2002) was introduced. Also from a high resolution stereo analysis, the slope, aspect and height data are extracted. Secondary information such as the canopy height is calculated combining such landcover information and the normalised DEM.

3.1 IKONOS RPC updating

IKONOS Geo products normally have 15-metre CE90 positioning accuracy (Space Imaging, 2005). This means that the sensor model needs to be updated to derive accurate 3D data.

RPCs (Rational Polynomial Coefficients) are provided instead of physical sensor information with each IKONOS image. Therefore, the first starting point in IKONOS stereo processing is to update the RPCs. A detailed specification for RPCs is fully described in the Earth Image Geometry models of the Open GIS abstract specification (Open GIS Consortium, 2001). In brief, RPCs use a ratio of two polynomial functions to transform ground X, Y and Z coordinates to image row and column number as follows:

$$r_1 = \frac{p_1}{q_1} \qquad (1)$$

$$c_1 = \frac{p_2}{q_2}$$

where p_1, p_2 are the numerators of the RPCs and q_1, q_2 are the denominators of the RPC.

Usually the format of a generic polynomial can be given as:

$$p = \sum_{i=0}^{m1}\sum_{j=0}^{m2}\sum_{k=0}^{m3} a_{ijk} X n^i Y n^j Z n^k \qquad (2)$$

where a_{ijk} is the polynomial coefficient in i,j,k order, X_n is the x ground coordinate, Y_n is the y ground coordinate and Z_n is the elevation of the ground level above a reference surface.

Grodecki and Dial (2003) proposed using a bundle block adjustment of RPC but a simpler method employed here is the RPC update with only 2 constant terms as Hanley et al. (2002) proposed. A bias corrected RPC uses the following relationships:

$$r + A_o + A_1 r + A_2 c = \frac{p_1(X,Y,Z)}{p_2(X,Y,Z)} \qquad (3)$$

$$c + B_o + B_1 r + B_2 c = \frac{p_3(X,Y,Z)}{p_4(X,Y,Z)}$$

where $A_o, ... B_2$ are the bias factors, (r,c) are the image row and column and $p1,..p4$ are the RPCs.

Therefore bias-corrected RPCs, incorporating shift terms A_0, B_0 can be given by:

$$p_1(X,Y,Z) = (a_1 - b_1 A_o) + (a_2 - b_2 A_o)X + ... + (a_{20} - b_{20} A_o)Z^3$$

$$p_3(X,Y,Z) = (c_1 - d_1 B_o) + (c_2 - d_2 B_o)X + ... + (c_{20} - c_{20} B_o)Z^3$$

$$(4)$$

We tested the accuracy of bias-corrected RPCs with GPS measurements which are provided by the University of Melbourne. As seen in Table 1, the positioning accuracy is within a maximum of 1-2 pixels in any IKONOS image. This implies that this accuracy is sufficient for accurate enough co-registration between stereo derived height points and the IKONOS multi spectral image.

Image name (Number of GCPs=23, number of Check points=12)	RMS error of check points		Max of checks shift	
	X	Y	X	Y
Left stereo image (po162796_pan0000000)	0.859	0.833	1.754	3.159
Right stereo image (po162796_pan0001000)	0.925	0.734	1.818	2.604
Multi-spectral image (po162775_pan0001000)	1.065	0.717	2.811	2.077

Table 1. Errors of bias compensated RPC

3.2 Stereo DSM extraction

The starting point of our IKONOS stereo DSM extraction is the exploitation of epi-polarity. Unfortunately, the IKONOS stereo in Hobart area is not rectified along epi-polar lines and the generic sensor information doesn't exist. We therefore used indirect epi-polar resampling, based on parallel projection (Morgan et al., 2004). With this method, the epi-polarity can be derived from the initial equation

$$G_1 c_l + G_2 r_l + G_3 c_r + G_4 r_r = 1 \quad (5)$$

where (c_l, r_l) and (c_r, r_r) are the image coordinates of corresponding tie points which can be manually or automatically selected.

Then, the coordinates in the epi-polar rectified image can be found by the transformations as below

$$\begin{bmatrix} c_{nl} \\ r_{nl} \end{bmatrix} = \frac{1}{s}\begin{bmatrix} \cos\theta_l & \sin\theta_l \\ -\sin\theta_l & \cos\theta_l \end{bmatrix}\begin{bmatrix} c_l \\ n_l \end{bmatrix} + \begin{bmatrix} 0 \\ -\frac{\Delta r}{2} \end{bmatrix} \quad (6)$$

$$\begin{bmatrix} c_{nr} \\ r_{nr} \end{bmatrix} = s\begin{bmatrix} \cos\theta_r & \sin\theta_r \\ -\sin\theta_r & \cos\theta_r \end{bmatrix}\begin{bmatrix} c_r \\ n_r \end{bmatrix} + \begin{bmatrix} 0 \\ \frac{\Delta r}{2} \end{bmatrix}$$

where (c_n, r_n) is the coordinate of epi-polar rectified image and (c,r) is the original image coordinate. The scale factor S, rotational angle θ and shift value Δr can be derived from the coefficients $G1$-$G4$. The details of this process and theory can be found in Morgan et al., (2004).

Since the target area is a very steep area where the height range is almost 1100m, even after making epi-polar rectified image pair by the indirect transformation, the x-disparity range, which is consequently the search area in image matching process, is likely to be too large. This problem was addressed by introducing a hierarchical rectification and improved RPC. Combining 1) and 5), **the** initial estimated coordinates of (c_{nl}, r_{nl}) and (c_{nr}, r_{nr}) can be calculated if there is a normalized coordinate of Z_n which can be taken from an existing initial DEM (GEODATA 9 in here). For the full exploitation of this scheme, we adopt a matching system. The improved DEM, which is hierarchically extracted from the GEODATA 9 is also applied with the RPC. Then the search range for the next level image matcher can be estimated. The Zitnick and Kanade (2001) algorithm (hereafter referred to as ZK) was introduced

for the matching of the epi-polar rectified image pairs. At each hierarchical level, the search area range becomes narrower resulting in a smaller window for the ZK image matcher. The output x-disparity ZK algorithms with resampled optical image pair is interpolated and used for the seed points generation of the UCL in-house Gruen's Adaptive Least Squared Correlation (ALSC) (Gruen, 1985) for the extraction of the final disparity. The effect of this method is shown in Figure 1.

Using this method, the consistency for global optimisation is guaranteed and the discontinuities in the urban area was successfully addressed.
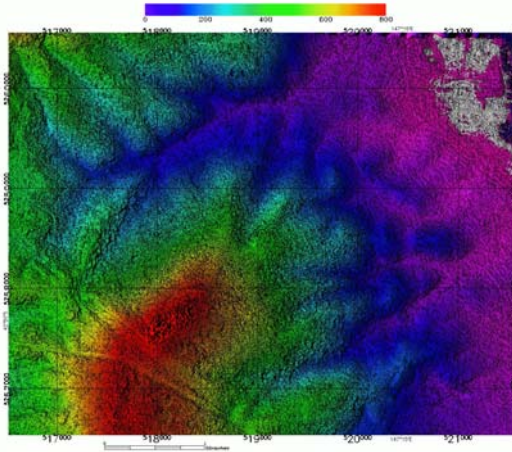

Figure 1. Stereo IKONOS DEM over test area (2m/pixel resolution)

For the object boundary delineation in urban areas, we once more applied Okutomi and Kanade (1992)'s image matching algorithm on the sub-area, which is classified as the urban area by the process described in 3.4. The disparity map from the ZK image matcher is then fed in this step as the initial disparity values in order to define an adaptive window size

3.3 DTM construction

Since the quality of height points are not high enough, (due to the lack of spatial resolution) especially with regard to landscape object boundary, "bare earth" DTM construction from stereo DSM is very challenging work. In the case of LiDAR DSM, the "flat seed areas" which don't include any landscape objects, can be defined by analysing slope and estimated maximum inland structure size (Muller et al. 2004). However, our stereo DSM includes very steep areas within the Hobart test area, and it is very difficult to find any flat areas using only slope analysis. Hence, we have defined the flat seed areas from an initial landcover classification. This is performed using a manual interpretation step wherein bare ground, grassland and roads are manually defined. A maximum likelihood classification is then performed using the multi-spectral orthorectified image which is re-sampled using the DSM produced using the method described in section 3.2. The initial flat seed mask was extracted by such classification process. A low pass filter was applied to the height points within this mask and a thin-plate-spline 3D surface is reconstructed from low-pass filtered height points. This surface is the initial DTM. Then by applying local minimum detection and region growing on n-DEM (DSM-DTM), the DTM can be updated hierarchically as previously described. It should be noted the DTM of this area, where there is dense forest and/or high slope topography, might not be very accurate (left bottom

area in Figure 2). This is a consequence of the low IKONNOS resolution, which can't detect the bare earth between the densely populated trees.
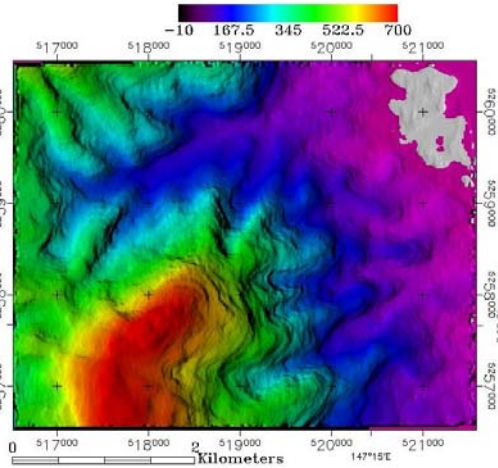

Figure 2. Bare Earth DTM (15m/pixel resolution)

3.4 Landcover classification

An extracted DTM using such a hierarchical approach as described above was employed to separate all the height points into "above-ground" and "at ground" components. The "above-ground" points can subsequently be separated into urban and forest classes using a NDVI mask. The NDVI difference for trees and buildings is usually significantly different such that the tree and building segmentation can be produced using either optimal thresholding or manual NDVI range assignment. It is then a very simple procedure to fuse 3D and optical data. The "at ground area" can be defined as the 'grassland' if it has high NDVI and "bare filled" if the NDVI value is lower than a pre-defined threshold value. This is a method to define reliable ground-truth for maximum landcover classifier. The result of next classification procedure is shown in Figure 3
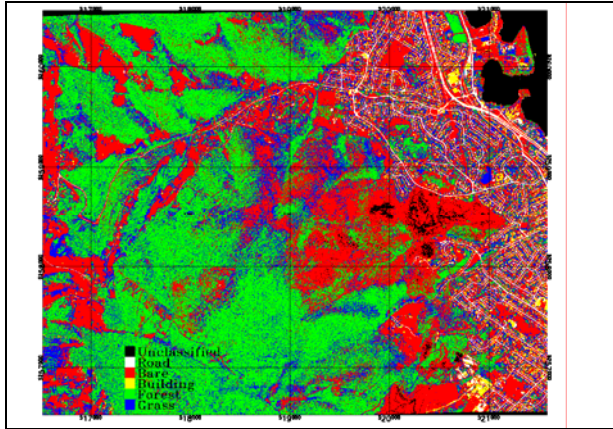
Figure 3. The original IKONOS image and landcover classification result for the Target area.

3.5 Individual object detection

With the classification processor, most of the necessary GIS data inputs, such as a DTM, landcover and the forest height, for the FARSITE model were extracted. However, some fire prediction tools also require the shape and location of individual objects to assess risk and behaviour of bushfires more precisely. Therefore the tree crown detection (>3-4m) method and the identification of individual houses were used with inputs from the normalised height points and multi-spectral information.

3.5.1 Buildings: Building footprint refinement and generalisation occur using simple processing of multi-spectral information. In the first stage, supervised classification is applied using the training vectors defined by NDVI together with 3D information. A 3D point distribution check is applied twice to fuse the results of the supervised classification with the segments produced by Fuzzy Clustering and Fuzzy Merging (FCFM) (Looney, 2002) of the multi-spectral image. Then a seeded region growing (SRG) method (Adams and Leanne, 1994) is applied to extract the correct building roof parts as shown in **Figure 4**. An algorithm for generating 3D building models is not developed here; instead, a simple boundary generalisation is performed. Further details can also be found in Muller et al. (2004).

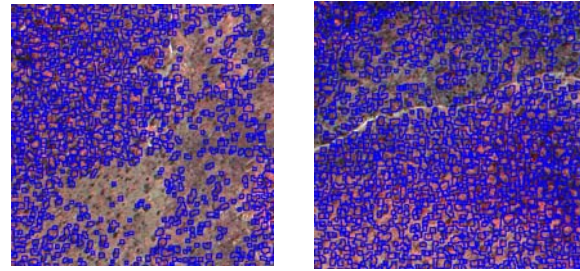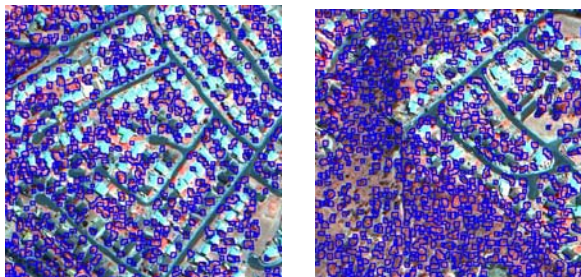Figure 4. The detected building footprints in housing areas

Figure 5. Tree detection process by morphological operation and ellipse fitting

3.5.2 Trees: This stage consists of three steps: supervised classification to discriminate grass and trees and individual tree crown splitting and fitting. The grass and tree splitting was already performed with a supervised classification and NDVI and the n-DEM based ground truth. Then within the tree area, the channel points between individual tree crowns' pixel intensity are detected by the method of Wood (1996). The next step comprises iterative morphological filtering and ellipse fitting (Fitzgibbon et al., 1996). By applying morphological erosion continuously around the channel points, the tree crown can be segregated. The remnant of these iterative operations is called the "core" of the tree crown and an ellipse can be fitted on the reconstructed boundary of the core. In our method, the eccentricity of fitted ellipses can be used as a verification parameter for the detected trees. If the fitted ellipses do not satisfy these criteria, then the failed part is used to provide feedback to unprocessed "preliminary" tree parts. Then the original crown shapes are reconstructed by morphological opening. The final result shows reasonable results in Figure 5. However, small shrub or young tree crowns in the bush as well as the individual tree crowns in very dense forest can't be clearly detected (or over-segmented) by this method. The reason is that the correct channel point detection in such small reflectance objects is barely possible at current IKONOS image resolutions. Therefore tree crown detection is performed with only sizeable (>2-3m radius) or isolated trees.

3.5.3 Evaluation : Ground truth of the target area is not available. Therefore the detected building and tree objects are compared with manually identified ones in sample areas. Table 2 shows the results of these evaluations.

|	TP	FP	FN	Detection Percentage	Branching Factor	Quality Percentage
Tree	230	34	48	82.733	0.147	73.717
Building	76	28	22	77.551	0.368	60.317

Table 2. The accuracy of tree and building objection result (Detection percentage=100TP/(TP+FN), Branching factor=FP/TP, Quality percentage=100TP/(TP+FP+FN), TP : True positive, FN : False negative, FP : False positive, Shufelt and McKeown (2003))

4. GIS ANALYSIS

Using the automated system described above, most of the bushfire parameters needed for prediction was extracted. Exceptions to this are the weather and the chemical or the moisture information on fuel For the non-available data such as detailed fuel types, moisture and weather, the default values extracted from average ground truth of the Hobart area were interpolated. **FARSITE**

(http://www.firemodels.org/content/view/112/143/) which is a fire behaviour and growth simulation system is employed. Then using the GIS data, two random ignition points were defined and the results of the simulations performed are shown in Figure 6.
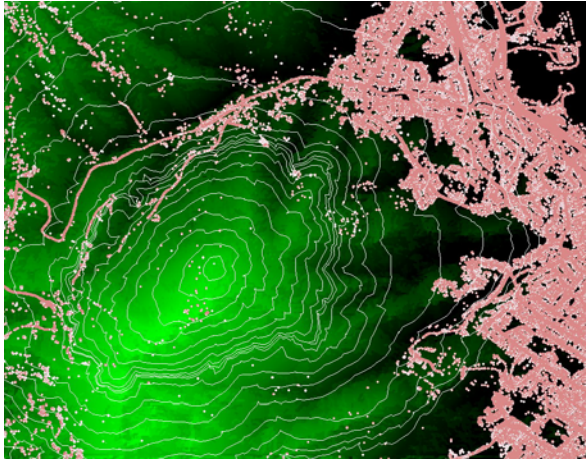
(a) Maximum fire spreading simulation (2007 August 8-11)
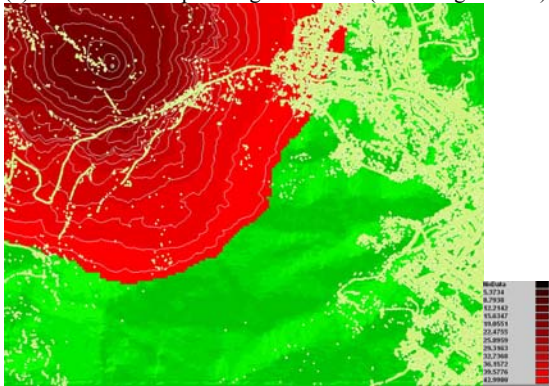
(b) Fireline intensity simulation (kW/m) (2007 July 7-8)

Figure 6. FIRSITE fire simulation results in test area.

5. CONCLUSION

The purpose of this work was to assess whether IKONOS stereo and multi-spectral imagery can be employed to provide suitable quality GIS data such as DTM, landcover classification as well as to identify individual objects for fire protection and behaviour simulator. The quality of DTM, landcover classification and individual object detection appeared to be adequate for such purpose. A DTM was derived with reasonable quality compared with results from a 250m resolution GEODATA 9 (max error < 10m) DTM. The quality of landcover classification is very reliable with visual comparison. Also, manual assessment indicates that the partial tree detection algorithm works well for calculating the fire spreading model. The detection ratios of buildings appear a lower than the tree detection result. However, considering the building sizes in the target area, which are mostly smaller than the big urban area, the algorithm appears to provide a good enough accuracy for fire risk assessment.
The FARSITE simulation results showed that these data sets which were mostly automatically extracted from IKONOS imagery works appear to work well with an existing fire combustion model.

Combined with ignition point detection using low resolution (MODIS) or medium resolution (ASTER) sensor, such schemes could greatly facilitate the decision making process to provide a more reliable, effective and robust system for bushfire prediction. Further algorithm development is required to identify different fuel types (vegetation types), assess moisture content from multi-spectral imagery and use more sophisticated data mining techniques for detailed object information such as 3D building shape detection and more reliable tree crowns for effective application of high resolution satellite data for bushfire risk assessment.

Reference

Adams, R., and Leanne, B. 1994. Seeded Region Growing. *IEEE Transaction Pattern Analysis and Machine Intelligence*. 16(6): 641-647.

Bureau of Meteorology Australia, 2003
http://www.bom.gov.au/info/leaflets/bushfire_weather.pdf

Chen, K., and McAneney, J. 2004, Quantifying bushfire penetration into urban areas in Australia, 31, L12212, doi:10.1029/2004GL020244,

Day, T., Cook, A. C., and Muller, J-P. 1992. Automated Digital Topographic Mapping Techniques for Mars. *International Archives of Photogrammetry and Remote Sensing*. 29(B4): 801-808.

Emergency Management Austalia 2006,
http://www.ema.gov.au/ema/emadisasters.nsf/c85916e930b93d50ca256d050020cb1f/85a9da8814839b4cca256d3300057b9e?OpenDocument (accessed 04 Apr. 2007)

Emergency Management Austalia 2006,
http://www.ema.gov.au/ema/emadisasters.nsf/c85916e930b93d50ca256d050020cb1f/271ae1df56d2f777ca256d3300057e41?OpenDocument (accessed 04 Apr. 2007)

Fitzgibbon, A. W., Pilu, M., and Fisher, R. B. 1996. Direct Least Squares Fitting of Ellipses. *IEEE Transactions on Pattern Analysis and Machine Intelligence*. 21(5): 476-480.

Geoscience Australia, 2005
http://www.ga.gov.au/image_cache/GA4783.pdf (accessed 04 Apr. 2007)

Grodecki , J. and Dial. G. 2003. Block adjustment of high-resolution satellite images described by rational functions," *Photogramm. Eng. Remote Sensing.*, 69(1): 59–68.

Gruen, A. 1985. Adaptive Least Squares Correlation: A powerful Image Matching Technique. *South Africa Journal of Photogrammetry, Remote Sensing and Cartography*. 14(3): 175-187.

Hanley, H. B., Yamakawa, T., and Fraser, C. S. 2002. Sensor Orientation for High Resolution Satellite Imagery. *Pecora 15/Land Satellite Information IV/ISPRS Commission I/FIEOS 10-15 November 2002, Denver, Colorado US,*
http://www.isprs.org/commission1/proceedings/paper/00090.pdf (Accessed 10 January 2005).

Looney, C. G. 2002. Interactive Clustering and Merging with a New Fuzzy Expected Value. *Pattern Recognition*. 35(11): 2413-2423.

Morgan, M., Kim, K., Jeong, S., and Habib, A. 2004, Indirect Epipolar resamping of Scenes Using Parallel Projection Modelling of Linear Array Scanners. *ISPRS-Congress 2004,12-23 July 2004, Istanbul, Turkey*

Muller, J-P., Kim, J. R., and Kelvin, J. 2004. Automated 3D Mapping of Trees and Buildings and its Application to Risk Assessment of Domestic Subsidence in The London Area. *ISPRS-Congress 2004,12-23 July 2004, Istanbul, Turkey*

Okutomi, M., and Kanade, T. 1992. A Locally Adaptive Window for Signal Matching. *International Journal of Computer Vision*. 7(2): 143-162.

Open GIS Consortium, 2001. Open GIS Abstract Specification - Topic 7: The Earth Imagery Case. https://portal.opengeospatial.org/files/?artifact_id=7467 (Accessed 1 April 2005).

Space Imaging.,2005. http://www.spaceimaging.com/whitepapers_pdfs/IKONOS_Product_Guide.pdf

Wood, J. 1996. The Geomorphological Characterisation of Digital Elevation Models. *Ph.D. Dissertation at the Department of Geography, University of Leicester.*

Zitnick, C. I., and Kanade, T. 2000. A Cooperative Algorithm for Stereo Matching and Occlusion Detection. *IEEE Transaction Pattern Analysis and Machine Intelligence 22(7), 675-684.*